Isokinetic TWC Evaporator Probe: Calculations and Systemic Uncertainty Analysis

Craig R. Davison[1]
National Research Council Canada, Ottawa, ON, Canada, K1A 0R6

J. Walter Strapp[2]
Met Analytics, Aurora, *ON, Canada L4G 4Y1*

Lyle Lilie[3]
Science Engineering Associates, Tolland, CT, 06084

Thomas P. Ratvasky[4]
NASA Glenn Research Center, Cleveland, OH, 44135-3191

Christopher Dumont[5]
FAA William J. Hughes Technical Center, Atlantic City, NJ, 08405

A new Isokinetic Total Water Content Evaporator (IKP2) was downsized from a prototype instrument, specifically to make airborne measurements of hydrometeor total water content (TWC) in deep tropical convective clouds to assess the new ice crystal Appendix D icing envelope. The probe underwent numerous laboratory and wind tunnel investigations to ensure reliable operation under the difficult high altitude/speed/TWC conditions under which other TWC instruments have been known to either fail, or have unknown performance characteristics and the results are presented in a companion paper[1]. This paper presents the equations used to determine the total water content (TWC) of the sampled atmosphere from the values measured by the IKP2 or necessary ancillary data from other instruments. The uncertainty in the final TWC is determined by propagating the uncertainty in the measured values through the calculations to the final result. Two techniques were used and the results compared. The first is a typical analytical method of propagating uncertainty and the second performs a Monte Carlo simulation. The results are very similar with differences that are insignificant for practical purposes. The uncertainty is between 2% and 3% at most practical operating conditions. The capture efficiency of the IKP2 was also examined based on a computational fluid dynamic simulation of the original IKP and scaled down to the IKP2. Particles above 24 μm were found to have a capture efficiency greater than 99% at all operating conditions.

Nomenclature

A	=	area
C_d	=	discharge coefficient
d	=	diameter
ϵ	=	expansion coefficient
FS	=	full scale

[1] Research Officer, Aerospace, AIAA Senior Member.
[2] Physical Scientist, Met Analytics Inc.
[3] President, Science Engineering Associates.
[4] Aerospace Engineer, Icing Branch, AIAA Senior Member.
[5] Research Engineer, Propulsion & Aircraft Icing Section, AIAA Senior Member.

γ = ratio of specific heats
η = efficiency
IKF = isokinetic factor
IKP = isokinetic total water content probe
IWC = ice water content
L = characteristic length
M = moles
m = mass (kg)
$\dot{m}$ = mass flow (kg/s)
μ = viscosity
ω = mass mixing ratio (mass of water per mass of dry air, g/g)
Ω = molar mixing ratio (moles of water per mole of dry air) in parts per thousand
Ω_{wet} = wet molar mixing ratio or mole fraction (moles of water per mole of dry air plus water vapor) in parts per thousand. This is the value provided by the IKP2 hygrometer.
p = pressure (Pa)
R = radius
R_{dry} = ideal gas constant for dry air
r_e = effective radius
Re = Reynolds number
ρ = density (kg/m^3)
Stk = Stokes number
T = temperature (K)
τ_f = flow time
τ_p = particle relaxation time
TWC = total water content (liquid and ice) (g/m^3)
u = uncertainty
V = speed (m/s)
v = volume (m^3)
$\dot{v}$ = volume flow (m^3/s)

Subscripts
amb = ambient condition
f = fluid
h = hydrometeors – solid and liquid particles in the atmosphere
IK = isokinetic
inlet = at the inlet to the IKP
o = total or stagnation conditions
op = orifice plate
p = particle
T = total water conditions – background vapor and vaporized hydrometeors
TWC = total water content (liquid and ice)
v = virtual – indicates temperature has been modified top account for water vapor effect on density in the ideal gas equation of state

I. Introduction

In 2006, technical members of the Engine Harmonization Working Group concluded that existing in-situ ice water content (IWC) measuring instruments were inadequate to collect validation data for new proposed ice crystal regulations (FAA Code of Federal Regulations (CFR) Part 33, Appendix D and EASA Certification Specification (CS) 25, Appendix P). It was decided to design and develop a new isokinetic total water content (TWC) evaporator (IKP) specifically for hostile high IWC environments. The original isokinetic TWC probe was developed by the National Research Council of Canada (NRC), Science Engineering Associates (SEA), and Environment Canada and tested at NRC, NASA, and Cox icing wind tunnel facilities[2,3,4,5,6,7].

In 2013, it was necessary to downsize the isokinetic probe so that it could be used on the Service des Avions Français Instrumentés pour la Recherche en Environnement (SAFIRE) Falcon-20 aircraft. This effort, led by Science Engineering Associates under NASA contract, and partnered with NRC who produced the flow path,

resulted in the second version of the probe (IKP2). The challenging requirements were to develop a new isokinetic evaporator probe, based on the original, which measured up to 10 g/m^3 at 200 m/s while reducing the power consumption, weight, and drag by roughly 50% to meet the SAFIRE Falcon-20 load limitations. Additionally, the instrument had to interface with existing mechanical hardware and wiring on the Falcon-20. A partner paper to this one presents in more detail the downsizing effort, and the development and testing performed to validate the probe for the flight campaigns[1].

This paper examines the equations used to determine the total water content (TWC) of the sampled atmosphere from the values measured by the IKP2, combined with ancillary data required from other instruments. The uncertainty in the final TWC is determined by propagating the uncertainty in the measured values through the calculations to the final result. Two techniques are used and the results compared. The first is a typical analytical method of propagating uncertainty and the second performs a Monte Carlo simulation. The capture efficiency of the IKP2 is also examined based on a computational fluid dynamic (CFD) simulation of the original IKP and scaled down to the IKP2.

II. Calculations

This section presents the equations used within the IKP2 software to calculate the TWC. Calculation of TWC requires inputs from sensors within the IKP2 and from external sensors providing airspeed, pressure, temperature and ambient background water vapor. The required inputs are summarized in Table 1. Several constant or property values are also required and are summarized in Table 2.

Table 1: Summary of inputted measurements

Variable	Description	Source	Uncertainty
T_{op}	Temperature at the orifice plate	IKP2	±1°C
p_{op}	Absolute pressure at the orifice plate	IKP2	±36 Pa (±0.026% FS)
Δp_{op}	Pressure change measured across the orifice plate	IKP2	±15 Pa (±0.111% FS)
$\Omega_{T,wet}$	Wet molar H_2O mixing ratio measured by IKP2 including evaporated liquid and solid water and background water vapor in parts per thousand	IKP2	±1.5% of reading
T_{amb}	Static temperature of the atmosphere being sampled	External	±1°C
p_{amb}	Static pressure of the atmosphere being sampled	External	±100 Pa
Ω_{amb}	Molar H_2O mixing ratio of the atmosphere being sampled	External	±1.5% of reading
V_{amb}	Speed of the air relative to the IKP2 (True Airspeed)	External	±2 m/s

Table 2: Summary of constants and air properties

Variable	Description	Source	Uncertainty
d_{inlet}	IKP2 inlet diameter	Measured	See text
μ_{op}	Viscosity at orifice plate	Calculated	Depends on condition
C_d	Orifice plate discharge coefficient	Calibration	±0.0033
R_{dry}	Ideal gas constant for dry air (287.1 J/kg-K)	Referenced	Assumed correct
γ	Ratio of specific heats (1.4)	Referenced	Depends on condition
d_{op}	Orifice plate diameter	Measured	Not required
d_{pipe}	Pipe leading to orifice plate diameter	Measured	Not required

A. Orifice Plate Mass Flow

The airflow through the IKP2 is measured with an ASME style orifice plate. The orifice plate was built as per the American Society of Mechanical Engineers (ASME) standard[8] with the following conditions and exceptions:

1) Pipe diameter of 18 mm - the standard covers down to 50 mm pipe diameter.
2) Upstream straight pipe of 22 diameters – standard does not cover these inlet conditions but a minimum between 13 and 25 diameters is likely required based on other upstream geometries that could provide similar downstream fluid dynamic conditions.

As the orifice plate was not built to the ASME standard[8] the discharge coefficient was calibrated to accurately determine the mass flow. This was done with a calibrated flowmeter (Omega FMA-1613A) and will be discussed in the error section. The density at the orifice plate is calculated with Eqs. (11) and (12) inserting the conditions at the orifice plate. The mass flow through an ASME orifice plate is given by Eq. (1). Substituting in the known

geometry the Eq. simplifies to (2). The discharge coefficient is a linear function of Reynolds number to the power of -0.75 in the standard ASME equation. The resulting equation for the discharge coefficient from the calibration is given by Eq. (3). The expansion coefficient accounts from the compressibility effects and is given Eq. (4) as per the ASME standard. When the geometry of the orifice plate is applied this reduces to Eq. (5) which is used in Eq. (2). The Reynolds number (Re) used in Eq. (3) is based on the usual Eq. given in (6). When the speed is replaced with the relationship between speed and mass flow and the geometry of the orifice plate applied Eq. (7) results. Since the Reynolds number depends on mass flow the calculation of mass flow becomes iterative. To solve for mass flow Eqs. (2), (3) and (7) were iterated 5 times.

$$\dot{m}_{op} = \frac{C_d}{\sqrt{1-\left(\frac{d_{op}}{d_{pipe}}\right)^4}} \epsilon \frac{\pi}{4} d^2 \sqrt{2\Delta p_{op} \rho_{op}} \tag{1}$$

$$\dot{m}_{op} = 0.0002275 C_d \epsilon \sqrt{\Delta p_{op} \rho_{op}} \tag{2}$$

$$C_d = 20.843 Re^{-0.75} + 0.681 \tag{3}$$

$$\epsilon = 1 - \left(0.41 + 0.35\left(\frac{d_{op}}{d_{pipe}}\right)^4\right)\frac{\Delta p_{op}}{\gamma p_{op}} \tag{4}$$

$$\epsilon = 1 - 0.50939\frac{\Delta p_{op}}{\gamma p_{op}} \tag{5}$$

$$Re = \frac{\rho_{op} V_{op} d_{pipe}}{\mu_{op}} \tag{6}$$

$$Re = \frac{4\dot{m}_{op}}{\pi d_{pipe} \mu_{op}} = \frac{70.6\dot{m}_{op}}{\mu_{op}} \tag{7}$$

$$\mu_{op} = -3.4211 \times 10^{-11}(T_{op} - 273.15)^2 + 5.0275 \times 10^{-8}(T_{op} - 273.15) + 1.7232 \times 10^{-5} \tag{8}$$

B. Isokinetic Factor

To minimise the distortion of the streamlines at the inlet and maximise the capture efficiency the mass flow entering the probe is maintained at the same level as would be passing through that area in the freestream. This mass flow is given by Eq. (9). The density is calculated using the ideal gas equation of state given in Eq. (11). The mass based mixing ratio is obtained by substituting the ambient water vapor as a mole fraction into Eq. (17). A virtual temperature is used to account for the water vapor present in the air and calculated with Eq. (12). This equation is derived from the ideal gas equation of state and the law of partial pressures as shown by Rogers and Yau[9]. The air flow is measured after the evaporator and includes the water vapor from the hydrometeors. At the inlet however the hydrometeors are in either solid or liquid state and do not significantly contribute (less than 0.001%) to the volume flow so this mass needs to be removed when measured determining the isokinetic factor (IKF). The hydrometeor mass flow is given by Eq. (13) and the resulting mass flow at the orifice plate due to air at the inlet is given by Eq. (14). This is combined with the isokinetic mass flow from Eq. (10) to obtain the IKF given by Eq. (15). The control system aims to maintain this value at 1.

$$\dot{v}_{inlet} = V_{amb} A_{inlet} \tag{9}$$

$$\dot{m}_{IK} = \dot{v}_{inlet} \rho_{amb} \tag{10}$$

$$\rho = \frac{p}{R_{dry} T_v} \tag{11}$$

$$T_v = T\left(\frac{1 + \frac{\omega}{0.622}}{1 + \omega}\right) \tag{12}$$

$$\dot{m}_h = \dot{v}_{inlet} \frac{TWC_{measured}}{1000} \tag{13}$$

$$\dot{m}_{op,air} = \dot{m}_{op} - \dot{m}_h \tag{14}$$

$$IKF = \frac{\dot{m}_{op,air}}{\dot{m}_{IK}} \tag{15}$$

C.Calculation of Total Water Content

The water vapor within the flow path of the IKP2 and the ambient (background) water vapor are measured using separate LICOR LI-840A CO_2/H_2O Gas Analyzers. The first step to obtain the TWC is to convert the mole fraction provided by the Licor humidity instrument to the mixing ratio with Eq. (16). The mole fraction is the moles of water vapor over the total moles (i.e. dry air plus water vapor) while the mole mixing ratio is the moles of water vapor over the moles of dry air. Eq. (17) converts the mole mixing ratio to the mass mixing ratio and accounts for the fact that the Licor value is in parts per thousand and the mixing ratio has dimensionless units of $g_{water\ vapor}/g_{dry\ air}$. Since no additional dry air was added between the inlet and the orifice plate the ambient mixing ratio can be subtracted from the mixing ratio at the orifice plate to give the mixing ratio of the hydrometeors, as shown and demonstrated by Eq. (18). The TWC is the mass of hydrometeors per mass of moist ambient air and is given by the first line of Eq. (19). The subsequent lines of Eq. (19) demonstrate its validity. The 1000 in the equation is to convert from kg in the density term to g in the TWC term. To convert the measured TWC to the actual ambient TWC an adjustment is required for the IKF. For the IKP2 geometry, at typical sampling speeds and particle sizes, most of the particles will continue directly into the probe even if the streamlines are not straight (i.e. the probe is not operating isokinetically). This is discussed in section IV below. If the probe is operating super isokinetically (i.e. is drawing in more air than required) then the true water content will be diluted; conversely if the probe is operating sub-isokinetically less air will be entering and the probe will overestimate the TWC. If we assume that all the hydrometeors go directly into the probe then multiplying by the isokinetic factor, as given by Eq. (20), will correct for the dilution or concentration of hydrometeors. Davison et al. present experimental results of correcting the TWC in this way for an IKP with the same inlet diameter and similar inlet geometry[10]. From an IKF=0.88 to 1.03 the corrected TWC matched within the variability of the test tunnel.

$$\Omega_T = \frac{\Omega_{T,Wet}}{1 - \Omega_{T,Wet}/1000} \tag{16}$$

$$\omega_T = \Omega_T \frac{MW_{water}}{1000 MW_{air}} = \Omega_T \frac{18.02}{1000(28.97)} = 6.220 \times 10^{-4} \Omega_T \tag{17}$$

$$\omega_{TWC} = \omega_T - \omega_{amb} = \frac{m_{amb\ vapour} + m_{hydrometeors}}{m_{dry\ air}} - \frac{m_{amb\ vapour}}{m_{dry\ air}} = \frac{m_{hydrometeors}}{m_{dry\ air}} \tag{18}$$

$$\begin{aligned} \mathrm{TWC}_{\mathrm{measured}} &= 1000 \rho_{\mathrm{amb}} \frac{\omega_{\mathrm{TWC}}}{1 + \omega_{\mathrm{amb}}} \\ &= 1000 \frac{\mathrm{m}_{\mathrm{dry\ air}} + \mathrm{m}_{\mathrm{amb\ vapor}}}{\mathrm{v}_{\mathrm{dry\ air}} + \mathrm{v}_{\mathrm{amb\ vapor}}} \frac{\frac{\mathrm{m}_{\mathrm{hydrometeors}}}{\mathrm{m}_{\mathrm{dry\ air}}}}{\frac{\mathrm{m}_{\mathrm{dry\ air}}}{\mathrm{m}_{\mathrm{dry\ air}}} + \frac{\mathrm{m}_{\mathrm{amb\ vapor}}}{\mathrm{m}_{\mathrm{dry\ air}}}} \\ &= 1000 \frac{\mathrm{m}_{\mathrm{dry\ air}} + \mathrm{m}_{\mathrm{amb\ vapor}}}{\mathrm{v}_{\mathrm{dry\ air}} + \mathrm{v}_{\mathrm{amb\ vapor}}} \frac{\mathrm{m}_{\mathrm{hydrometeors}}}{\mathrm{m}_{\mathrm{dry\ air}} + \mathrm{m}_{\mathrm{amb\ vapor}}} \\ &= 1000 \frac{\mathrm{m}_{\mathrm{hydrometeors}}}{\mathrm{v}_{\mathrm{dry\ air}} + \mathrm{v}_{\mathrm{amb\ vapor}}} \end{aligned} \tag{19}$$

$$\mathrm{TWC} = \mathrm{TWC}_{\mathrm{measured}} \cdot \mathrm{IKF} \tag{20}$$

III. Uncertainty Analysis

To examine the uncertainty in the final TWC value the uncertainty in the underlying inputs must first be determined. They must then be combined to determine the resulting total uncertainty. The standard technique which assumes normal distributions of uncertainties will first be applied. Subsequently, a Monte Carlo analysis will be performed to more realistically determine the uncertainty at a range of the conditions. This technique does not assume normal distributions in the original uncertainties and can produce a non-normal distribution in the final uncertainty.

A. Orifice Plate

The orifice plate uncertainty is the most complicated as it relies on many parameters. The simplest to quantify are those of the transducers. The quoted uncertainty on the pressure transducer and temperature measurement are given in Table 1. To improve the accuracy of the orifice plate mass flow measurement it was calibrated against an accurate commercial flowmeter with known accuracy. Uncertainties in the measurement of the orifice plate size or slight inconsistencies with the static pressure port production will be compensated for in the discharge coefficient generated through the calibration procedure. To obtain the discharge coefficient 18 points were measured across the operating range of Reynolds numbers for the orifice plate. The uncertainty in the resulting curve fit gives an uncertainty in the discharge coefficient of ±0.0033. This is the value provided in Table 2. Error is introduced through the calculation of the Reynolds number from Eq. (7). The value of 70.6 is based on known constants and geometric area and any error in this value will be accounted for in the discharge coefficient calibration. Interestingly the uncertainty in the discharge coefficient depends on the uncertainty in the mass flow which due to the iterative calculation depends on the uncertainty in the discharge coefficient, but the primary sources of uncertainty in the mass flow calculation are the measured parameters of absolute pressure and temperature used to calculate density and pressure change across the orifice. The ratio of specific heats also varies depending on temperature and water vapor. It can vary from 1.4 by up to 0.35% under normal operating conditions (dry air to 0.024 g H_2O/g dry air at 70°C).

Returning to the Reynolds number, the error in the viscosity can be significant. The curve fit Eq. (8) matches the viscosity for dry air[11] within 0.05% across the pressure and temperature range of operation. However, the effect of water vapor on viscosity has also been ignored. The method of Tsilingiris was used to calculate the viscosity of humid air and compared to the results obtained from Eq. (8)[12]. At the maximum water vapor that the hygrometer can measure this results in a 4.2% error. At lower water vapor more realistic of actual conditions the error is around 1%. As will be shown in the following section this error is insignificant in the final calculation of TWC.

B. Isokinetic Factor

The uncertainty in the isokinetic factor depends on the uncertainty in the measured mass flow and the external parameters of airspeed, static pressure and temperature. Typical uncertainty values for aircraft data are quoted in Table 1 and used in the analysis. The diameter of the inlet is required to get the area and was determined using pins in increments of 0.0025 mm with an uncertainty of 0.0010 mm. The pin inserted determines the minimum size of the inlet (since it goes in) and the next pin size up that does not fit determines the maximum size of the inlet. Therefore the uncertainty in the inlet is uniformly distributed between the pin size that fits and the larger pin size that does not as described by the expression below where pin n fits into the inlet:

$$d_{pin,n} \pm u_{pin} \leq d_{inlet} \leq d_{pin,n+1} \pm u_{pin}$$

The water vapor measurements and TWC also enter into the equations and will be discussed in the following section. The ideal gas constant is assumed to be correct as any error in it will be insignificant compared to the other uncertainties.

C. Total Water Content

The ultimate objective of the IKP2 is to determine the TWC. The uncertainty in the TWC depends on the uncertainties discussed above and the measured water vapor. The ambient water vapor also directly impacts the TWC. As the accuracy and uncertainty of the ambient water vapor often depend more on the sampling system than the instrument, it is discussed in more detail in the companion paper by Strapp et al[1]. For this paper, the uncertainty of the ambient water vapour is assumed to be the same as the instrument uncertainty used in the IKP2.

D. Analytical Calculation of Uncertainty

Uncertainties can be combined using the traditional technique presented by Kline and McClintlock[13]. This method requires the uncertainty in each parameter to be normally distributed The general equation to combine uncertainties is given by (21) for dependent variable y which is a function of independent variables x_1 to x_n with associated uncertainties u_1 to u_n. The following sections will apply this equation to those outlined above resulting in an analytical calculation of the uncertainty in the TWC value.

$$u_y = \left[\left(\frac{\partial y}{\partial x_1}u_1\right)^2 + \left(\frac{\partial y}{\partial x_2}u_2\right)^2 + \cdots + \left(\frac{\partial y}{\partial x_n}u_n\right)^2\right]^{0.5} \tag{21}$$

1. *Orifice Plate*

Combining Eqs. (2) and (5) and substituting Eq. (11) for density yields Eq. (22) for mass flow at the orifice plate. Applying Eq. (21) accounting for the uncertainty in C_d, $T_{v,op}$, p_{op}, and Δp_{op} yields Eq. (23). The uncertainty in the ratio of specific heats is ignored due to its weak influence on the result and small value. The virtual temperature is used in several locations and applying Eq. (21) to Eq. (12) yields Eq. (24). Obtaining the uncertainty in the mixing ratio from Eq. (25) and applying it to get the uncertainty in virtual temperature results in a u_{Tv}=1.04 K at the maximum water vapor of the LI-840A hygrometer and 1.01 K at a realistic maximum mass mixing ratio in flight (0.017 g/g) based on cloud measurements from three flight programs to date for temperatures colder than 0°C. A theoretical maximum mass mixing ratio of 0.025 g/g results in an u_{Tv}=1.02 K. As these are very close to the uncertainty in the temperature measurement, which is 1 K, the uncertainty in the virtual temperature will be assumed to be the uncertainty in the temperature.

The discharge coefficient has two sources of uncertainty. The first is from the calibration and is provided in Table 2. The second is from the uncertainty in the measurements that are required by Eq. (7) and subsequently by Eq. (3). Combining those two equations and applying Eq. (21), results in Eq. (26) Applying the worst case error in viscosity was taken as the uncertainty in viscosity. With the assumptions and approximations listed above, the uncertainty in the measured mass flow was determined.

$$\dot{m}_{op} = 0.002275 C_d \left(\frac{\Delta p_{op} p_{op}}{R_{dry} T_{v,op}}\right)^{0.5} - \frac{0.0001159 C_d}{\gamma}\left(\frac{\Delta p_{op}^3}{R_{dry} T_{v,op} p_{op}}\right)^{0.5} \tag{22}$$

$$u_{\dot{m}_{op}} = \left[\left(\left(0.002275\left(\frac{\Delta p_{op} p_{op}}{R_{dry} T_{v,op}}\right)^{0.5} - \frac{0.0001159}{\gamma}\left(\frac{\Delta p_{op}^3}{R_{dry} T_{v,op} p_{op}}\right)^{0.5}\right) u_{C_d}\right)^2 + \left(\left(\frac{-0.002275 C_d}{2}\left(\frac{\Delta p_{op} p_{op}}{R_{dry}}\right)^{0.5} T_{v,op}^{-1.5} + \frac{0.0001159}{2\gamma}\left(\frac{\Delta p_{op}^3}{R_{dry} p_{op}}\right)^{0.5} T_{v,op}^{-1.5}\right) u_{T_{op}}\right)^2 + \left(\left(\frac{0.002275 C_d}{2}\left(\frac{\Delta p_{op}}{R_{dry} T_{v,op}}\right)^{0.5} p_{op}^{-0.5} + \frac{0.0001159 C_d}{2\gamma}\left(\frac{\Delta p_{op}^3}{R_{dry} T_{v,op}}\right)^{0.5} p_{op}^{-1.5}\right) u_{p_{op}}\right)^2 + \left(\left(\frac{0.002275 C_d}{2}\left(\frac{p_{op}}{R_{dry} T_{v,op}}\right)^{0.5} \Delta p_{op}^{-0.5} - \frac{0.0003477 C_d}{2\gamma}\left(\frac{1}{R_{dry} T_{v,op}}\right)^{0.5} \Delta p_{op}^{0.5}\right) u_{\Delta p_{op}}\right)^2\right]^{0.5} \tag{23}$$

$$u_{T_v} = \left[\left(\frac{1 + {}^{\omega}/_{0.622}}{1+\omega} u_T\right)^2 + \left(T\left(\frac{0.6077}{(1+\omega)^2}\right) u_\omega\right)^2\right]^{0.5} \cong u_T \tag{24}$$

$$u_\omega = \frac{6.22 \times 10^{-4} u_{\Omega_{T,wet}}}{\left(1 - \frac{\Omega_{T,wet}}{1000}\right)^2} \tag{25}$$

$$u_{C_d} = \left[\left(\left(-0.642 \mu_{op}^{0.75} \dot{m}_{op}^{-1.75}\right) u_{\dot{m}_{op}}\right)^2 + \left(\left(0.642 \mu_{op}^{-0.25} \dot{m}_{op}^{-0.75}\right) u_{\mu_{op}}\right)^2 + u_{C_{d,calibration}}^2\right]^{0.5} \tag{26}$$

2. Isokinetic Factor

The isokinetic factor, given by Eq. (27), was be obtained by combining Eqs. (9) through (15). It has previously been shown that the difference in uncertainty between the actual and virtual temperature is negligible and Eq. (12) will be omitted resulting in Eq. (28) for uncertainty in IKF. The uncertainty in the TWC will be examined in the next section. Applying Eq. (21) to the equation for the area of a circle results in the uncertainty in the inlet area in terms of diameter given by Eq. (30). The value for the uncertainty in the area combines half the pin increment size with the uncertainty in the two pins used to determine the upper and lower limits as shown by Eq. (29).

$$IKF = \frac{R_{dry} T_{v,amb}\left(\dot{m}_{op} - V_{amb} A_{inlet} \frac{TWC_{measured}}{1000}\right)}{V_{amb} A_{inlet} p_{amb}} \tag{27}$$

$$u_{IKF} = \left[\left(\left(\frac{R_{dry} T_{v,amb}}{p_{amb} V_{amb} A_{inlet}} \right) u_{m_{op}} \right)^2 + \left(\left(\frac{-\dot{m}_{op} R_{dry} T_{v,amb}}{p_{amb} V_{amb}^2 A_{inlet}} \right) u_{V_{amb}} \right)^2 + \left(\left(\frac{-\dot{m}_{op} R_{dry} T_{v,amb}}{V_{amb} A_{inlet}^2 p_{amb}} \right) u_{A_{inlet}} \right)^2 + \left(\left(\frac{-R_{dry} T_{v,amb}}{1000 p_{amb}} \right) u_{TWC_{measured}} \right)^2 + \left(\left(\frac{-R_{dry} T_{v,amb} \left(\dot{m}_{op} - V_{amb} A_{inlet} \frac{TWC_{measured}}{1000} \right)}{V_{amb} A_{inlet} p_{amb}^2} \right) u_{p_{amb}} \right)^2 + \left(\left(\frac{R_{dry} (\dot{m}_{op} - V_{amb} A_{inlet} \frac{TWC_{measured}}{1000})}{V_{amb} A_{inlet} p_{amb}} \right) u_{T_{amb}} \right)^2 \right]^{0.5} \tag{28}$$

$$u_{d_{inlet}} = \left(2u_{pin}^2 + \left(\frac{d_{pin,n+1} - d_{pin,n}}{2} \right)^2 \right)^{0.5} = 1.92 \times 10^{-6} \, [m] \tag{29}$$

$$u_{A_{inlet}} = \frac{\pi d_{in\,let}}{2} u_{d_{i\,nlet}} = 2.05 \times 10^{-8} \, [m^2] \tag{30}$$

3. Total Water Content

Combining Eqs. (11), (19) and (20) yields Eq. (31) for the TWC and applying Eq. (21) yields Eq. (32) for the uncertainty. The uncertainty in the measured TWC is required to determine the uncertainty in the IKF. The measured TWC is the TWC without correcting for the IKF and the uncertainty is given by Eq. (33).

$$TWC = \frac{1000 IKF p_{amb}}{R_{dry} T_{v,amb}} \left(\frac{\omega_T - \omega_{amb}}{1 + \omega_{amb}} \right) \tag{31}$$

$$u_{TWC} = \left[\left(\left(\frac{1000 p_{amb} IKF}{R_{dry} T_{v,amb} (1+\omega_{amb})} \right) u_{\omega_T} \right)^2 + \left(\left(\frac{1000 p_{amb} (\omega_T - \omega_{amb})}{R_{dry} T_{v,amb} (1+\omega_{amb})} \right) u_{IKF} \right)^2 + \left(\left(\frac{1000 IKF (\omega_T - \omega_{amb})}{R_{dry} T_{v,amb} (1+\omega_{amb})} \right) u_{p_{amb}} \right)^2 + \left(\left(\frac{-1000 IKF p_{amb} (\omega_T - \omega_{amb})}{R_{dry} T_{v,amb}^2 (1+\omega_{amb})} \right) u_{T_{v,amb}} \right)^2 + \left(\left(\frac{-1000 p_{amb} IKF (1+\omega_T)}{R_{dry} T_{v,amb} (1+\omega_{amb})^2} \right) u_{\omega_{amb}} \right)^2 \right]^{0.5} \tag{32}$$

$$u_{TWC_{measured}} = \left[\left(\left(\frac{1000 p_{amb}}{R_{dry} T_{v,amb} (1 + \omega_{amb})} \right) u_{\omega_T} \right)^2 + \left(\left(\frac{1000 (\omega_T - \omega_{amb})}{R_{dry} T_{v,amb} (1 + \omega_{amb})} \right) u_{p_{amb}} \right)^2 + \left(\left(\frac{-1000 p_{amb} (\omega_T - \omega_{amb})}{R_{dry} T_{v,amb}^2 (1 + \omega_{amb})} \right) u_{T_{v,amb}} \right)^2 + \left(\left(\frac{-1000 p_{amb} (1 + \omega_T)}{R_{dry} T_{v,amb} (1 + \omega_{amb})^2} \right) u_{\omega_{amb}} \right)^2 \right]^{0.5} \tag{33}$$

E. Numerical Calculation of Uncertainty

The second technique to ascertain the uncertainty was to perform a Monte Carlo analysis. In this technique the result from the IKP2 was calculated as discussed in the Calculations section. The set of possible "true" results was then determined by varying the input values based on the uncertainties in Table 1 and Table 2. Uncertainties on instruments were assumed to be normally distributed. The inlet diameter was varied by determining an upper and lower pin size based on the pin uncertainty (assumed normally distributed) and then obtaining the diameter from a uniform distribution between those two sizes. The viscosity in the "true" set was calculated for humid air using the technique of Tsilingiris, discussed above[12]. The ratio of specific heats for the actual temperature and water vapor was calculated with the method of Bucker et al. instead of assuming a value of 1.4.[14]

For each test case 10^5 simulations were run and the results, less the IKP2 result, were sorted in ascending order. The confidence interval was then directly extracted from the ordered values. For the 95% confidence interval the lower bound is the 2,500th value and the upper bound the 97,500th value. To check that sufficient simulations were run ten identical cases were run and the confidence intervals compared. For TWC, the lower bound varied from -1.93% to -1.95% and the upper bound from 1.66% to 1.67%. This variation was considered small enough even on a small sample size of ten.

F. Results

A set of test cases were examined to determine the uncertainty in the IKP2 across a range of operating conditions, including both flight and wind tunnel operation. For flight conditions, altitudes of 12.19 km (40 kft), 9.14 km (30 kft) and 6.10 km (20 kft) corresponding to static temperatures of -42°C, -29°C and -10°C (corresponding to international standard atmosphere (ISA) +15°C) and static pressures of 18.7 kPa, 30.1 kPa and 46.6 kPa were examined. A constant indicated air speed of 121 m/s (235 knots) was assumed, which corresponded to true airspeeds of 252 m/s (490 knots), 204 m/s (397 knots) and 171 m/s (331 knots), for the three different altitudes respectively. At each altitude the following TWCs were tested: 15, 10, 5, 4, 3, 2, 1, 0.5 and 0.1 g/m^3. The 15 g/m^3 value was chosen as it corresponds to the maximum calibrated water vapor in the IKP2 hygrometer. The 10 g/m^3 was chosen as it was the original IKP2 design point. The remaining values were chosen to cover a realistic range of operation. At each condition the background atmosphere was assumed to be saturated over ice.

Figure 1 shows the analytical percentage uncertainty in the final TWC measurement as a function of TWC. Above 9.14 km, which corresponds to -29°C, and above a TWC of 0.5 g/m^3 the uncertainty ranges from 2% to 3%. At low altitude and low TWC the uncertainty increases to about 48%. This is due to the decreasing fraction of the water vapor measured in the IKP2 that contributes to the TWC, as shown by Figure 2. Figure 2 shows the uncertainties as a function of the fraction of water vapour from the hydrometeors over the total water vapour. The uncertainties at different altitudes collapse into one curve. Even with the addition of all other test points examined covering variations in IKF, ambient (background) water vapor and wind tunnel tests the main driver of uncertainty is the fraction of water vapor measured contributing to the TWC. The IKP2 has the least uncertainty when the background water vapor becomes zero. The uncertainty in the hygrometers is a fraction of the water vapor value rather than of full scale. As the fraction of the water vapor in the IKP contributing to the TWC decreases the uncertainty becomes a larger fraction of the TWC portion. The uncertainty in the ambient water vapor also becomes a larger fraction of the TWC reading and is combined into the uncertainty as shown in Eq. (32). In practice the uncertainty in the IKP2 and ambient humidity readings can be reduced by comparison and adjustment under known conditions. A discussion of these methods is provided by Strapp et al[1].

Table 3 shows the contribution of the terms in Eq. (32) to the overall uncertainty. At 12.9 km and 15.1 g/m^3 the ω_T and IKF terms dominate. At the lower, 0.50 g/m^3, level the terms all decrease with the decrease in TWC, except for the ω_{amb} term which remains almost constant, but it is still an order of magnitude below the larger terms. At the 6.1 km and 0.50 g/m^3 condition the ω_{amb} and ω_T terms increase by orders of magnitude due to the higher level of ambient water vapour at the warmer condition, but the TWC has remained constant from the higher colder condition. The contribution of the other terms becomes insignificant at this condition.

Table 3: Contribution of individual terms from Eq. (32) to analytical uncertainty in TWC

Conditions		Terms in Eq. (32)					u_{TWC} (g/m^3)
Altitude	TWC (g/m^3)	ω_T (g/m^3)^2	IKF (g/m^3)^2	p_{amb} (g/m^3)^2	$T_{v,amb}$ (g/m^3)^2	ω_{amb} (g/m^3)^2	
12.2 km (40 kft)	15.1	6.2×10^{-2}	3.8×10^{-2}	6.5×10^{-3}	4.3×10^{-3}	2.6×10^{-6}	0.33
12.2 km (40 kft)	0.50	8.2×10^{-5}	4.0×10^{-5}	7.1×10^{-6}	4.7×10^{-6}	2.3×10^{-6}	0.012
6.1 km (20 kft)	0.50	1.7×10^{-3}	5.5×10^{-5}	1.2×10^{-6}	3.6×10^{-6}	1.1×10^{-3}	0.054

The effect of varying the IKF was also examined. As the IKF decreases, the uncertainty also decreases. It is assumed that the hydrometeors continue to enter the probe as if the flow was isokinetic. So as the air flow goes down, the concentration of hydrometeors goes up, reducing the uncertainty caused by the background water vapor as discussed above. However, the gain due to reduced IKF is negligible. The uncertainty in TWC only decreases from 2.51% to 2.44% for an IKF change from 1.1 to 0.9 at 1 g/m^3 and 9.14 km. This increase is smaller than the uncertainty in the assumed capture efficiency of 1, so this is not a viable method to decrease the uncertainty. Any larger deliberate reductions in the target IKF value are of course undesirable due to possible saturation at low flow values[1], and increasing errors for small particle measurement due to non-isokinetic sampling.

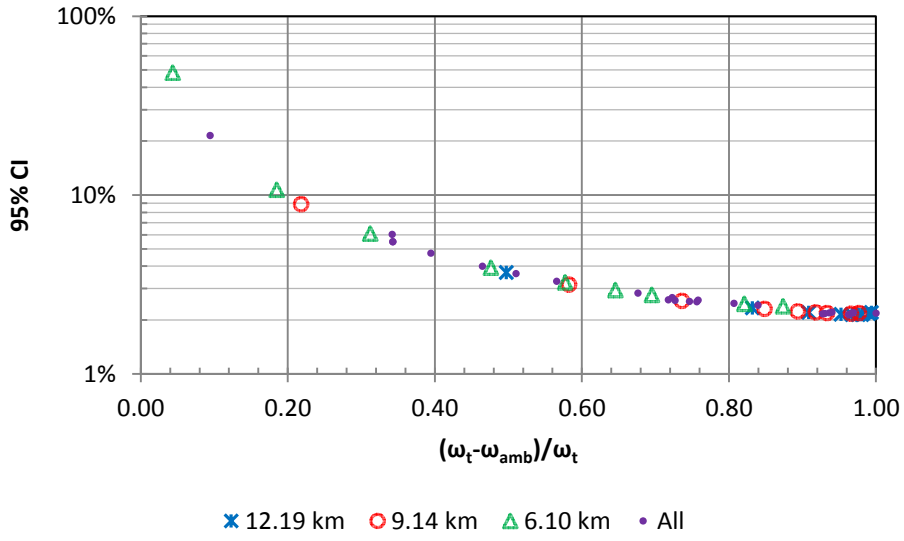

Figure 1: Analytical percent uncertainty in TWC at 3 altitudes and from 0.1 to 15 g/m^3

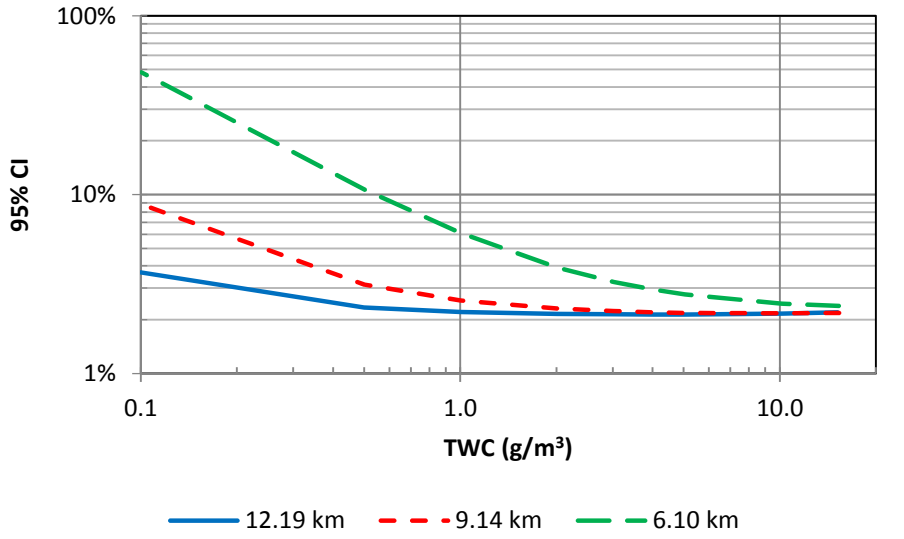

Figure 2: Analytical percent uncertainty in TWC at 3 altitudes and from 0.1 to 15 g/m^3 as a function of fraction of water vapor measured by the IKP2 that contributes to the TWC

Typical wind tunnel conditions were also examined. Total temperature of -10°C and total pressure of 101.325 kPa, true airspeed of 150 m/s (292 knots) and saturated air at static conditions were considered. These conditions are representative of a recirculating tunnel such as the Icing Research Tunnel at NASA Glenn, but conservative for tunnels such as the Research Altitude Test Facility (RATFac) and M7 Test Cell 5 at the National Research Council of Canada which do not recirculate and may not reach saturation. This means that the uncertainty created by the ambient background water vapor term is smaller. Earlier calculations for flight conditions assumed saturation over ice, but this test was examining a typical liquid icing tunnel so saturation over liquid was assumed. Figure 3 shows the increasing uncertainty as the TWC decreases. The uncertainty rapidly increases below 0.5 g/m^3, reaching about 22% at 0.1 g/m^3, but is almost constant over 1 g/m^3. The effect of relative humidity of less than 100% is examined in Figure 4. The uncertainty more than doubles when the background relative humidity increases from 0 to 100%. This affect would be greater at warmer temperatures, allowing for higher background water vapor mixing ratios.

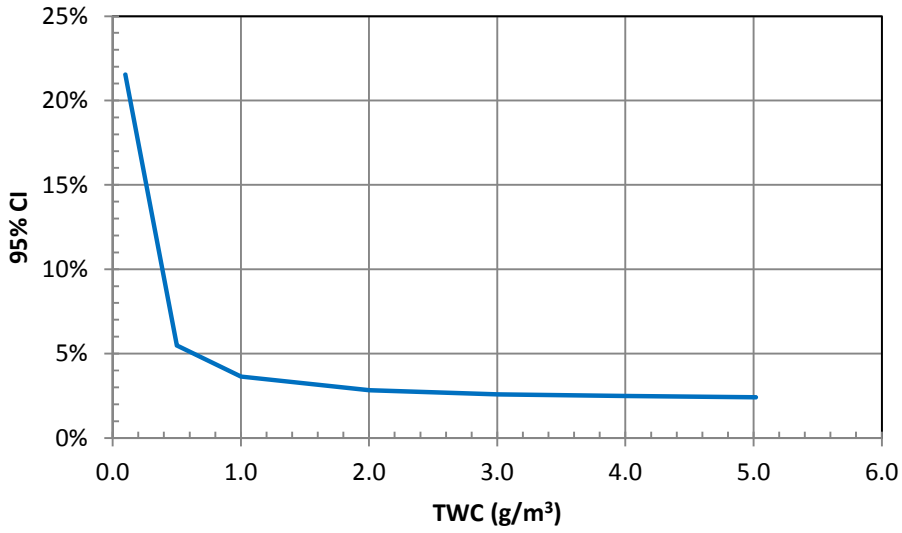

Figure 3: Uncertainty under typical recirculating wind tunnel conditions (T_o=-10°C, p_o=101.325 kPa, V=150 m/s, saturated over liquid at static conditions)

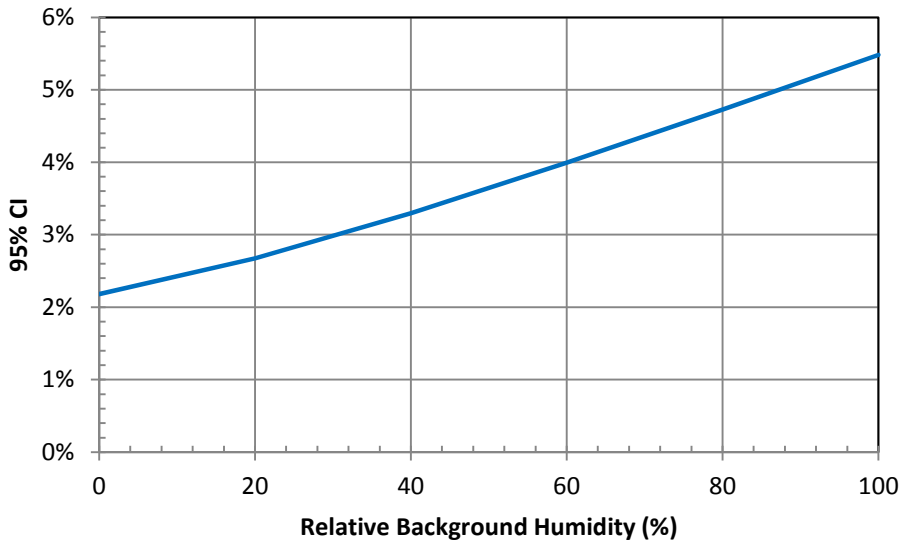

Figure 4: Uncertainty under wind tunnel conditions with varying background water vapor (T_o=-10°C, p_o=101.325 kPa, V=150 m/s, TWC=0.5 g/m^3)

The difference between the analytical and numerical determination of uncertainty is small and of academic rather than practical significance. Due to the small variations $1x10^6$ numeric simulations were run for each test case. Figure 5 shows the ratio of the numerical over analytical uncertainty. The analytical uncertainty is equal in magnitude for both the upper and lower bounds. The numerical uncertainty, however, does not require this to be true. At the low water content the uncertainties approach each other. At the 0.1 g/m^3 value the numerical upper confidence interval approaches the analytical but does not reach it. At higher values of TWC both the upper and lower numerical uncertainty bounds decrease with respect to the analytical. The numerical uncertainty eliminated some conservative assumptions included in the analytical calculations. The inclusions of non-normal uncertainties in the numerical simulation, such as the viscosity of humid air and the inlet area, contribute to the unbalanced confidence interval.

While the mean of the numerically calculated uncertainty is not zero, the distribution is nearly normal. Figure 7 shows the uncertainty distribution at 12.90 km (40 kft) and 15 g/m^3 TWC. The numerical distribution is based on binning of the test cases while the analytical is calculated by using the standard deviation and mean of the final uncertainty to generate a normal distribution. A higher concentration around zero uncertainty is apparent in the numeric simulation as is the reduced uncertainty on the upper bound. Figure 6 shows the 9.14 km case at 5 g/m^3 TWC. As the normally distributed background water vapor uncertainty begins to dominate the mean of the uncertainty in TWC comes closer to zero. However, the reduced uncertainty on the upper bound in the numerical simulation is still apparent, as is the overall reduced uncertainty demonstrated by a larger fraction at zero uncertainty.

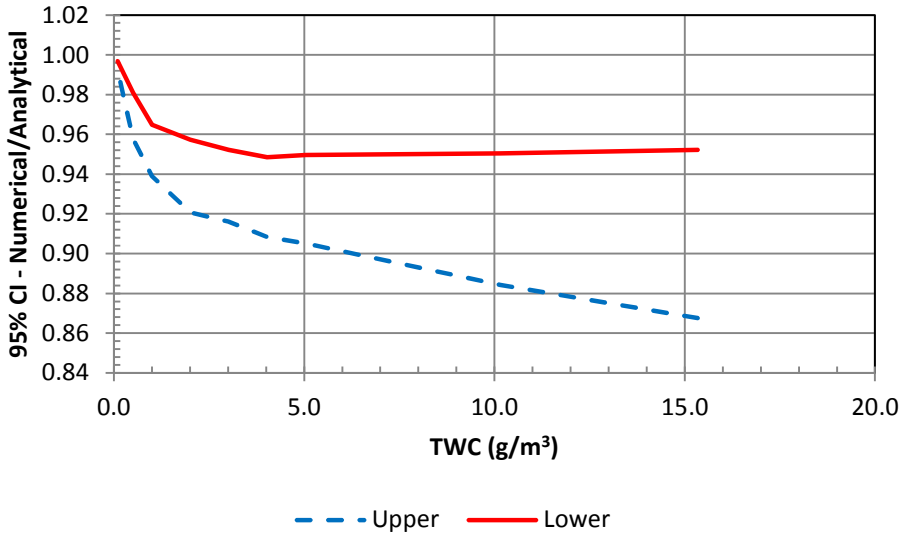

Figure 5: Comparison of numerical and analytical confidence intervals for 9.14 km altitude

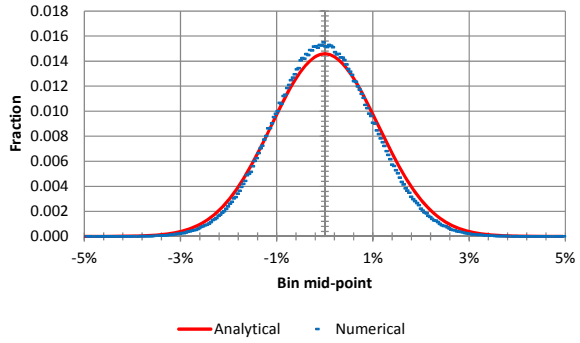

Figure 6: Distribution of analytical and numerical uncertainty for 9.14 km (30 kft) altitude and 5 g/m^3 TWC

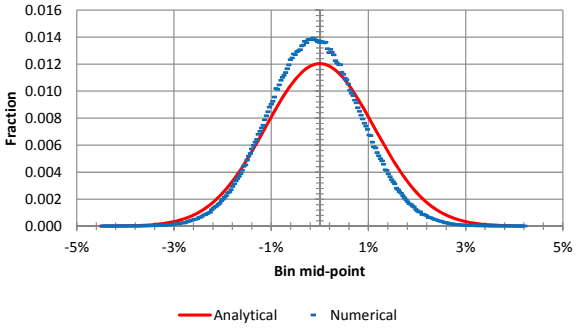

Figure 7: Distribution of analytical and numerical uncertainty for 12.19 km (40 kft) altitude and 15 g/m^3 TWC

IV. Collection Efficiency

The collection efficiency affects the accuracy of the TWC but is dependent on the size distribution of the particles being measured. Therefore, it should be considered separately from the uncertainty discussion above. The capture efficiency of the original, larger, IKP was determined from CFD simulations. The CFD results were correlated to Stokes number to extend to other operating conditions[2,15]. Details on the method and CFD can be found in the report by Davison et al[15]. For reference, the Stokes number is given in Eqs. (34) to (36) below. To approximate the collection efficiency of the new IKP2 the following technique was used.

The core flow into the IKP is relatively undisturbed and the reduction in particles entering the probe is caused by bending of the streamlines around the inlet. Therefore, any reduction in efficiency was assumed to be caused by a lack of particles in the ring at the outer radius of the inlet as represented in Figure 8. The radius R encompasses the entire inlet area. The radius r_e encompasses the equivalent area that would be required to achieve a given efficiency if it had a 100% capture efficiency and the area bounded by R and r_e had a zero capture efficiency. This means that the area bounded by r_e is the same percentage of the area bounded by R as the capture efficiency, as shown by Eq. (38).

It was assumed that for the same Stokes number both the original IKP and current IKP2 would have the same distance from the edge of the intake affected (R-r_e is the same) since the geometries were almost the same. This is given by Eq. (37). Eq. (38) was re-arranged to solve for r_e for both the new and original IKPs, substituted into Eq. (37) and solved to give Eq. (39) for the new capture efficiency. The characteristic length in Eq. (36) was scaled by 0.7 to compensate for the size reduction of the new probe.

$$\mathrm{Stk} = \frac{\tau_p}{\tau_f} \tag{34}$$

$$\tau_p = \frac{\rho_p d_p^2}{18\mu_f} \tag{35}$$

$$\tau_f = \frac{L}{V_f}; \quad L = 0.0105\ m \tag{36}$$

$$R_{original} - r_{e\ original} = R - r_e \tag{37}$$

$$\eta_{capture} = \frac{A_e}{A} = \frac{r_e^2}{R^2} \tag{38}$$

$$\eta_{capture} = \left(\frac{R_{original}\left(\sqrt{\eta_{capture\ original} - 1}\right) + R}{R} \right)^2 \tag{39}$$

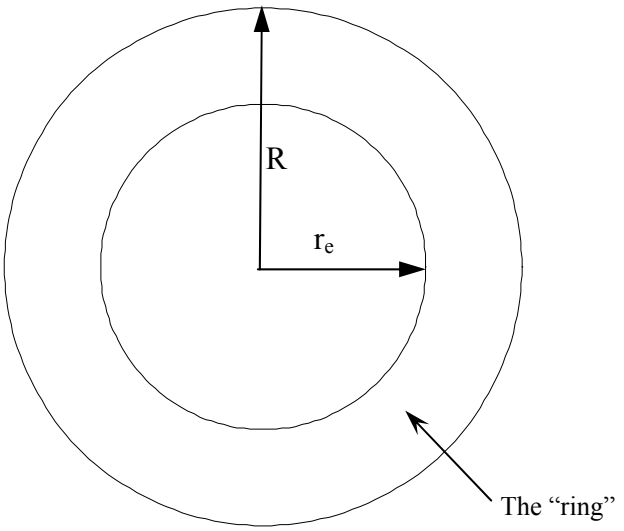

Figure 8: Representation of IKP2 inlet

Figure 9 compares the collection efficiency achieved for a given Stokes number for the original and new IKPs. The reduced area of the IKP2 reduces the collection efficiency at the lower Stokes numbers. Above a Stokes number of 10 the difference in efficiencies becomes negligible. Figure 10 provides the lines of constant Stokes number and efficiency with altitude. Any location above a given line will be higher than the efficiency for that line. This calculation assumed a constant indicated airspeed (IAS) of 121 m/s and a ISA temperature plus 15°C. The 99% efficiency line has a maximum size of 24 μm and is below 20 μm at altitudes where the IKP2 is likely to be used. Any particles above 9 μm will achieve a 95% collection efficiency. The line corresponding to a Stokes number of 0.15 is the worst case with the particles essentially following the air flow. Any reduction in size below this level does not change the collection efficiency. All particle sizes refer to a single particle size and not the average size of a distribution of particles. To determine the collection efficiency for a distribution would require summing the mass fraction of each size times the efficiency for that diameter.

Figure 11 shows the variation in collection efficiency due to a non-unity IKF. Above a Stokes number of 7 there is no significant change in efficiency with a variation in IKF from 1.05 to 0.95. This corresponds to a particle size of 10 μm at an altitude of 10.65 km and airspeed of 210 m/s and 20 μm at sea level and airspeed of 66 m/s. At lower Stokes numbers the efficiency increases for the super isokinetic condition, as the hydrometeors are vacuumed into the probe. Conversely, at sub-isokinetic conditions the efficiency is decreased, as hydrometeors are entrained in the airflow going around the inlet.

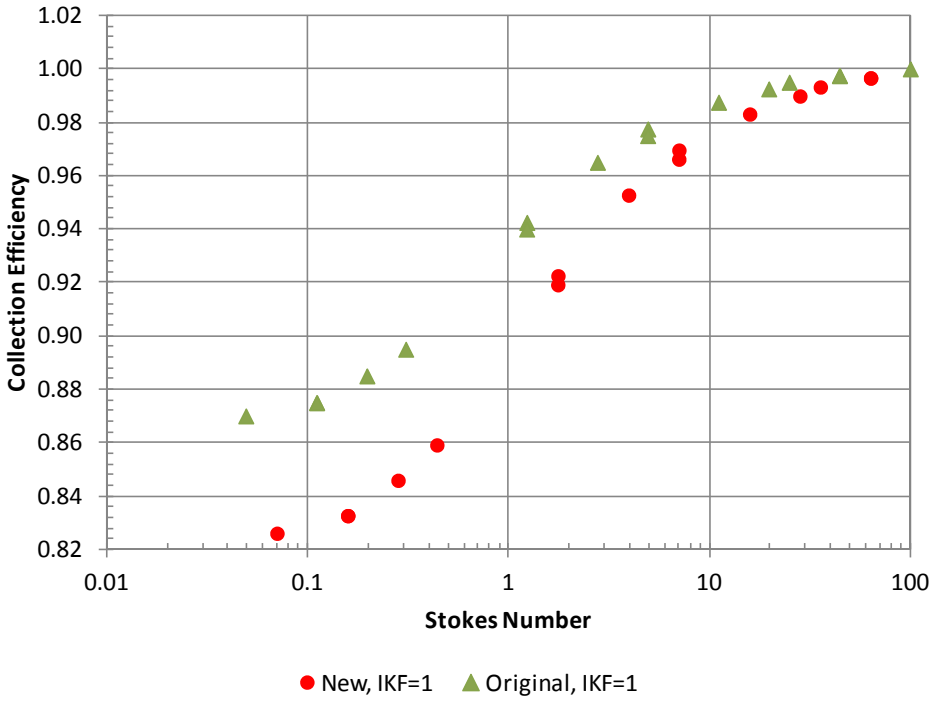

Figure 9: Calculated collection effciency for original IKP and the new IKP2 with Stokes number

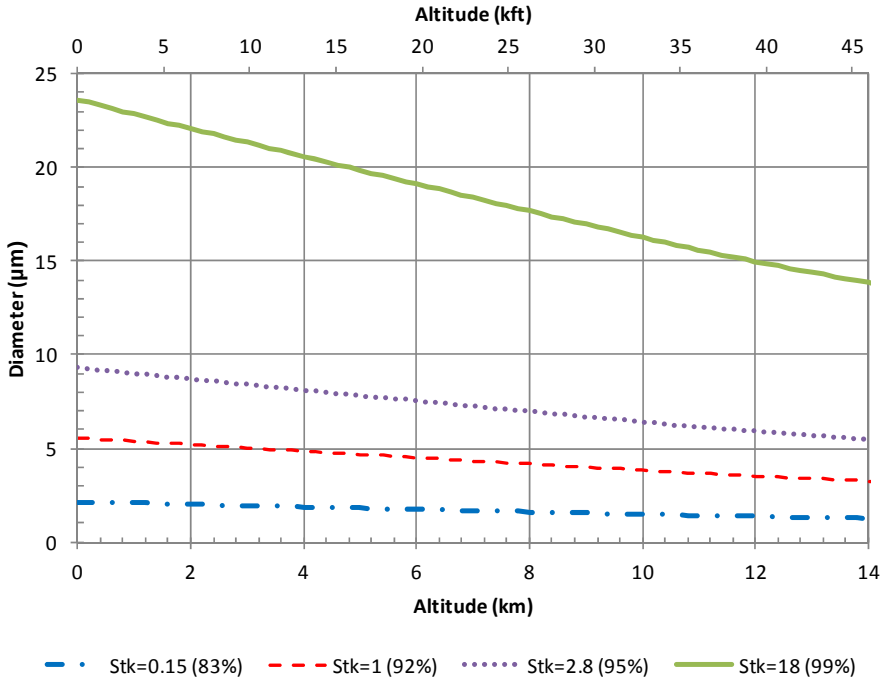

Figure 10: Ice diameter required to reach specified Stokes number and collection efficiency with increasing altitude at constant indicated airspeed of 121 m/s and hot atmosphere

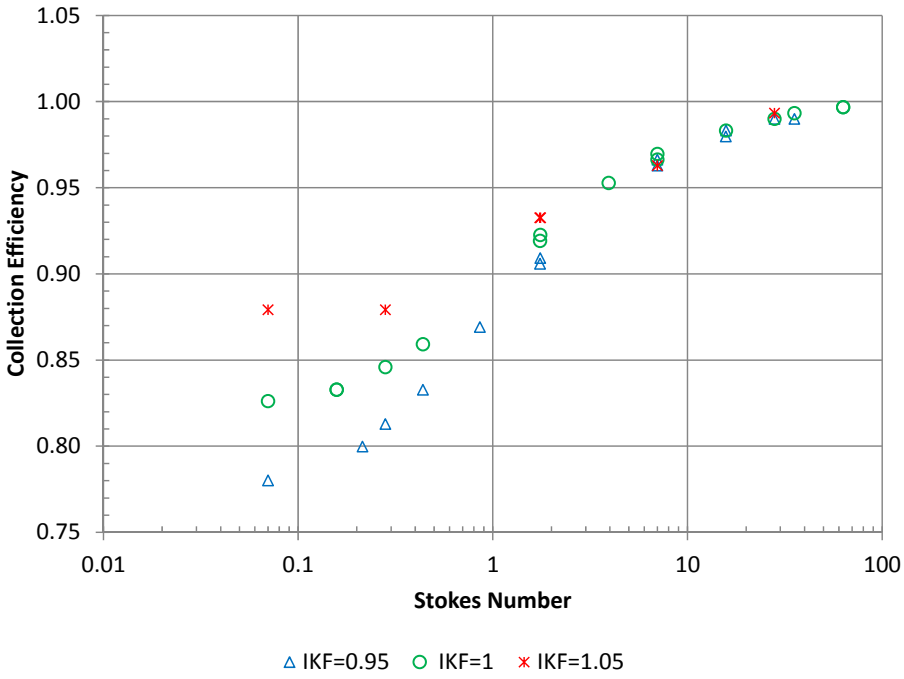

Figure 11: Variation in collection efficiency due to IKF

V. Conclusions

The uncertainty of the TWC value based on the listed uncertainties of the constituent measurements has been determined. During flight conditions below SAT=-29°C and TWC above 0.5 g/m^3 the uncertainty varies from 2% to 3% of the reading. As the background water vapor levels increase relative to the TWC the estimated uncertainty increases. The worst case occurs for the calculations at the warmest temperature and lowest TWC, where uncertainty is estimated at 50% at 0.1 g/m^3 and -10°C (u_{TWC}=0.05 g/m^3). The numerical calculation of uncertainties reveal confidence intervals slightly smaller than those resulting from the analytical calculations. They also reveal a bias towards a lower reading based on the uncertainties. The bias, however, was too small to be of practical significance. The capture efficiency was found to be greater than 99% for particles greater than 24 μm at sea level and greater than 15 μm at 12 km (40 kft).

Acknowledgments

Funding to support this project was provided by the Federal Aviation Administration, the NASA Aviation Safety Program, Environment Canada, and Transport Canada. Mr. Charles Landreville and Dr. Michael Benner of NRC; and Mr. Dan Bouley and Mr. Chris Sivo of SEA provided important technical support to the development of the IKP2. NRC is acknowledged for providing support for the writing of this paper.

References

[1.] Strapp, J. W., Lilie, L., Ratvasky, T. P., Davison, C. R., and Dumont, C., "Isokinetic TWC Evaporator Probe Development and Performance Testing for the HAIC-HIWC Darwin 2014 and Cayenne 2015 Field Campaigns", 2016, Submitted for publication, 8th AIAA Atmospheric and Space Environments Conference, June 17, 2016, Washington, DC.

[2.] Davison, C. R., Rutke, T., Strapp, J. W., Ratvasky, T. P., and Emery, E. F., "Naturally Aspirating Isokinetic Total Water Content Probe: Pre-flight Wind Tunnel Testing and Design Modifications", 2012, AIAA 2012-3040, 4th AIAA Atmospheric and Space Environments Conference, June 28, 2012, New Orleans, Louisana.

[3.] Davison, C. R., Ratvasky, T. P., and Lilie, L. E., "Naturally Aspirating Isokinetic Total Water Content Probe: Wind Tunnel Test Results and Design Modifications", 2011, 2011-38-0036, SAE 2011 International Conference on Aircraft and Engine Icing and Ground Deicing, June 17, 2011, Chicago, IL, SAE, USA.

[4.] Davison, C. R., MacLeod, J. D., and Ratvasky, T. P., "Naturally Aspirating Isokinetic Total Water Content Probe: Preliminary Test Results and Design Modifications", 2010, AIAA-2010-7530, 2nd AIAA Atmospheric and Space Environments Conference, Aug. 5, 2010, Toronto, ON, Canada, AIAA.

[5.] Davison, C. R. and MacLeod, J. D., "Naturally Aspirating Isokinetic Total Water Content Probe: Intake Deicing and Heat Transfer", 2009, AIAA-2009-3862, 1st AIAA Atmospheric and Space Environments, June 25, 2009, San Antonio, Texas.

[6.] Davison, C. R., MacLeod, J. D., and Strapp, J. W., "Naturally Aspirating Isokinetic Total Water Content Probe: Evaporator Design and Testing", 2009, AIAA-2009-3861, 1st AIAA Atmospheric and Space Environments, June 25, 2009, San Antonio, Texas.

[7.] Davison, C. R., MacLeod, J. D., Strapp, J. W., and Buttsworth, D. R., "Isokinetic Total Water Content Probe in a Naturally Aspirating Configuration: Initial Aerodynamic Design and Testing", 2008, AIAA Paper 2008-0435, 46th AIAA Aerospace Sciences Meeting and Exhibit, Jan. 10, 2008, Reno, Nevada.

[8.] American Society of Mechanical Engineers, "Measurement of Fluid Flow in Pipes Using Orifice, Nozzle and Venturi," ASME, Standard ASME MFC-3M-1989, New York, Jan. 1990.

[9.] Rogers, R. R. and Yau, M. K., *A Short Course in Cloud Physics*, 3rd ed., Pergamon Press 1989.

[10.] Davison, C. R., Landreville, C., and Benner, M., "Development and Validation of Compact Isokinetic Total Water Content Probe for Wind Tunnel Characterization", 2016, Submitted for publication, 8th AIAA Atmospheric and Space Environments Conference, June 17, 2016, Washington, DC.

[11.] Kadoya, K., Matsunaga, N., and Nagashima, A., "Viscosity and Thermal Conductivity of Dry Air in the Gaseous Phase," *Journal of Physical and Chemical Reference Data*, Vol. 14, No. 4, 1985, pp. 947-970.

[12.] Tsilingiris, P. T., "Thermophysical and transport properties of humid air at temperature range between 0 and 100°C," *Energy Conversion and Management*, Vol. 49, No. 5, 2008, pp. 1098-1110.

[13.] Kline, S. J. and McClintock, F. A., "Describing Uncertainties in Single-Sample Experiments," *Mechanical Engineering*, Vol. 75, No. 1, 1953, pp. 3-8.

[14.] Bucker, D., Span, R., and Wagner, W., "Thermodynamic Property Models for Moist Air and Combustion Gases," *Journal of Engineering for Gas Turbines and Power*, Vol. 125, No. 1, 2003, pp. 374-384.

[15.] Davison, C. R., Landreville, C., Mings, V., and Currie, T. C., "Phase 2 Development and Testing of Isokinetic Probe to Measure Total Water Content During Ground and Airborne Testing," National Research Council Canada, LTR-GTL-2014-0004, Ottawa, Mar. 2014.